ACS OMEGA

http://pubs.acs.org/journal/acsodf

Article

Enterobacter hormaechei-Driven Novel Biosynthesis of Tin Oxide Nanoparticles and Evaluation of Their Anti-aging, Cytotoxic, and Enzyme Inhibition Potential

Muhammad Rizwan,* Shah Faisal,* Muhammad Hamza Tariq, Sania Zafar, Ajmal Khan, and Farhan Ahmad

Cite This: *ACS Omega* 2023, 8, 27439−27449

Read Online

ACCESS | Metrics & More | Article Recommendations

ABSTRACT: Nanotechnology is a research hotspot that has gained considerable interest due to its potential inferences in the bioscience, medical, and engineering disciplines. The present study uses biomass from the *Enterobacter hormaechei* EAF63 strain to create bio-inspired metallic tin oxide nanoparticles (SnO_2 NPs). The biosynthesized NPs were extensively analyzed using UV spectroscopy, X-ray diffraction (XRD), scanning electron microscopy (SEM), energy-dispersive X-ray spectroscopy (EDX), and Fourier transform infrared (FTIR) techniques. The identification of the crystalline phase was confirmed by XRD. The SEM technique elucidated the morphological characteristics and size of SnO_2 NPs. SEM investigation revealed that the SnO_2 NPs have a size of 10 nm with spherical morphology. The capping of NPs was confirmed by FTIR analysis that revealed the presence of different compounds found in the biomass of the *E. hormaechei* EAF63 strain. Later, EDX confirmed the elemental composition of NPs. Moreover, the synthesized SnO_2 NPs were employed for important applications including anti-aging, anti-Alzheimer's, anti-inflammatory, anti-larvicidal, and antibacterial action against sinusitis pathogens. The highest value was observed for *Streptococcus pyogenes* (19.75 ± 0.46), followed by *Moraxella catarrhalis* (17.49 ± 0.82) and *Haemophilus influenzae* (15.31 ± 0.73), respectively. Among the used concentrations, the highest inhibition of 76.8 ± 0.93 for 15-lipoxygenase (15-LOX) was observed at 400 μg/mL, followed by 67.4 ± 0.91 for cyclooxygenase-1 (COX-1). So, as an outcome, *E. hormaechei*-mediated SnO_2 NPs might be considered as the safe and effective nanoplatforms for multifunctional biological applications in the field of nanomedicine.

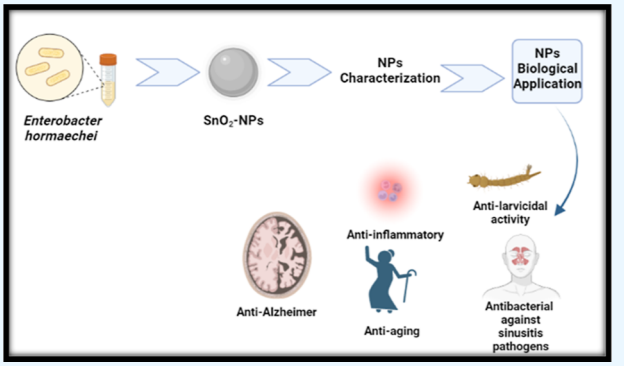

1. INTRODUCTION

Currently, in contrast to typical and commercial bulk materials, nano-oxides and nanoparticles (NPs) are intensively explored for their optoelectronic, electrical, magnetic, catalytic, and pharmacological characteristics.[1,2] As a consequence of all these distinctive attributes, investigators became fascinated to start working on nano-sized materials, including metal oxides, nanodots, nanotubes, and nanoemulsions.[3] It is clear from the literature that certain morphological characteristics, i.e., shape, size, and composition, significantly affect the properties of materials, including biological properties such as drug release, enzymatic inhibition, and targeted drug discovery with minimum side effects. NPs, in particular, have a large surface area to volume ratio, making them very effective in almost all fields of science.[4] Researchers mainly rely on physical and chemical processes for the synthesis of nanomaterials in the early era of nanotechnology. But these techniques are subject to environmental dangers, and mainly they are not biocompatible. To combat this issue, researchers are now focusing on switching toward the green synthesis of nanomaterials.[5]

NPs possess excellent biocompatibility, enhanced permeability, reduced toxicity, precise targeting, and enhanced stability, which make them more beneficial in comparison to other nanomaterials, such as layered materials.[6] Even for NPs, different materials are available, which can be used to synthesize them, among which, metal oxides are considered as the important ones owing to high transparency and conductivity. Among other metal oxides, tin oxide NPs (SnO_2 NPs) are one of the most effective ones for biomedical

Received: April 28, 2023
Accepted: June 14, 2023
Published: July 17, 2023

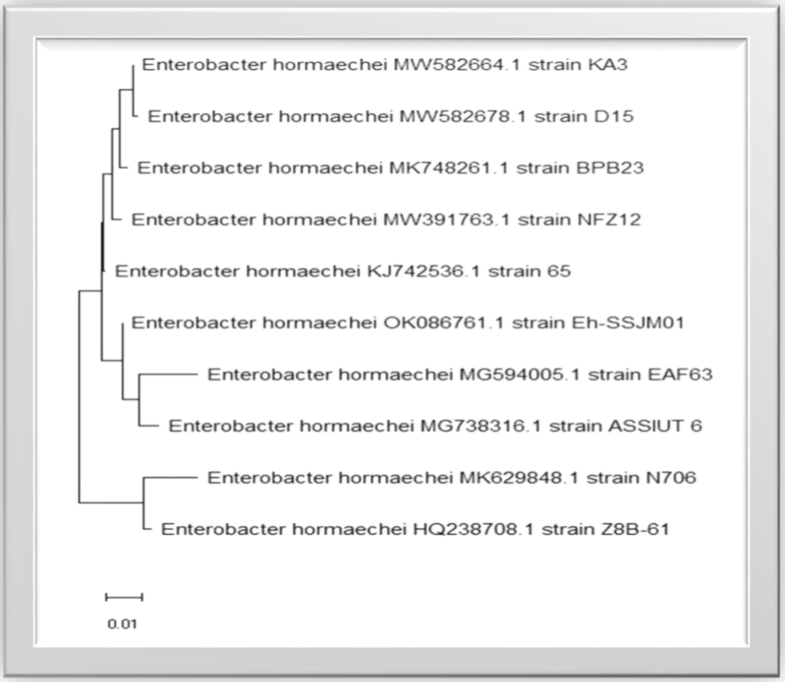

Figure 1. 16S rDNA sequence of the *E. hormaechei* EAF63 strain, which was used in the manufacturing of metallic SnO_2 NPs.

applications owing to their high surface to volume ratio, which assists them to scavenge free radicals easily and thus can be used for biological applications. It is because of this reason that SnO_2 NPs have been reported to possess antiviral, antibacterial, anticancer, antifungal, and drug delivery properties.[7] Until now, many physical and chemical approaches have been reported to prepare SnO_2 NPs; some of them are sol−gel, hydrothermal, solvothermal, chemical vapor deposition, and co-precipitation methods. However, all these methods have limitations like being expensive, poisonous, environmentally hazardous, and time-consuming. Therefore, scientists have been trying to find biological methods to replace the existing methods to overcome the aforementioned issues.[8] The most common biological methods used to synthesize NPs involve the use of medicinal plants or microorganisms. Microbes capture metal ions and trap them within bacterial cells, which reduce them through enzymatic reduction, followed by their capping for stabilization.[9] Previously, many bacterial strains have been used to synthesize NPs; however, there is no available data on *Enterobacter hormaechei*-mediated production of SnO_2 NPs, despite the fact that this bacterial strain has been reported to produce other biologically important NPs, such as silver NPs and zinc oxide NPs. Therefore, the current study is novel in such a way that it uses *E. hormaechei* as the bacteria to synthesize SnO_2 NPs, which are further tested for different biomedical-related applications, including anti-aging, anti-inflammatory, and cytotoxic potential.

2. RESULTS AND DISCUSSION

2.1. SnO_2 NPs' Synthesis. The bacteria were identified as *E. hormaechei* strain EAF63 based on the homology and alignments with previously known bacterial rDNA genomes (Figure 1), and the data was reported to the NCBI GenBank database (accession number MG594005.1). Nano-sized metallic oxides are known to be produced by various microbes.[10] Because the bacterial products control the morphology, size, and properties of the NPs, they have qualities like chemically produced materials. A considerable influence on the physical characteristics of NPs, such as size, shape, and crystallinity, is exerted by the microorganisms which have been used in the manufacturing process.[11] In the presence of bacterial biomass and metal salts, the production of white precipitates demonstrated the successful synthesis of SnO_2 NPs. When the 1 mM stannous chloride ($SnCl_2$) solution was introduced to the bacterial culture drop by drop, the tin ions were reduced, a white precipitate developed, and the reaction mixture changed color from colorless to white, confirming the production of SnO_2 NPs. The synthesis of NPs depends on where the NPs are produced; microbe-mediated synthesis may occur either intracellularly or extracellularly. Bio reduction happens on the exterior of bacterial/microbial cells during extra-cellular production in the vicinity of enzymes that are accessible somewhere at the membrane.[12−14] Metallic ions are also fascinated within the bacterial cell during intracellular biosynthesis, where they readily form SnO_2 NPs in the presence of enzymes. The Sn^{2+} ions are caught by extra-cellular enzymes generated by the microbial cell or membrane-linked aggregations of proteins on the exterior of the bacterial cell, and dehydrogenase enzymes begin the reduction process.[14,15] By acquiring the electron pair, Sn^{2+} ions are reduced, and a molecule of NADP is converted to NADH, resulting in the creation of extra-cellular Sn ions. The presence of structures resembling protein molecules on the surface was discovered using FTIR, and these molecules were thought to have a promising function in stabilizing SnO_2 NPs. In the synthesis process, a bio-based molecule (amino acids) also acts as a capping/stabilizing agent, reducing the need for hazardous chemicals. Figure 2 depicts a proposed process for the green production of SnO_2 NPs. The synthesized NPs are reported to be stable, even under visible light irradiation. Previously, it has

https://doi.org/10.1021/acsomega.3c02932
ACS Omega 2023, 8, 27439−27449

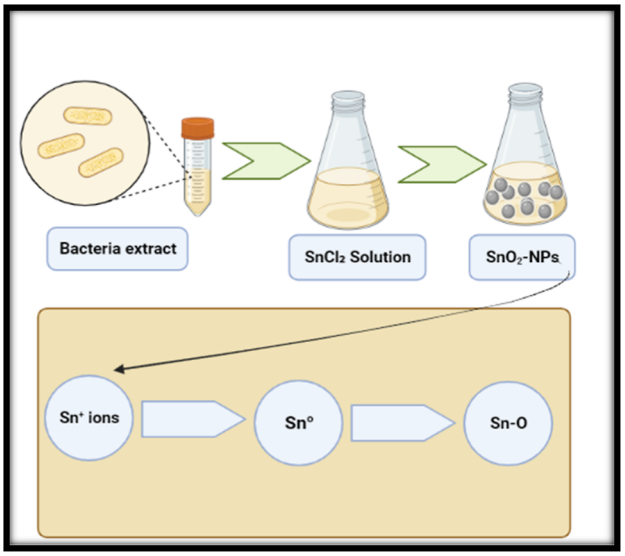

Figure 2. Mechanistic approach toward the synthesis of SnO_2 NPs.

been shown that the carbon sheath and nanointerface, once combined, help in improving the photocatalytic activity of materials by increasing the absorption ability and transfer efficiency of photogenerated carriers. The photocatalytic activity of SnO_2 NPs is due to their ability to absorb light and create electron−hole pairs, which can react with water or oxygen molecules in the surrounding environment to produce ROS such as a superoxide anion ($O_2^{\bullet-}$) and a hydroxyl radical ($^{\bullet}OH$). Furthermore, it has been proposed that the formation of ROS from SnO_2 NPs is mediated by the transfer of electrons from the conduction band of SnO_2 to oxygen molecules absorbed on the surface of the NPs. This results in the formation of superoxide anion radicals, which can then react with water to produce hydroxyl radicals. In summary, the generation of ROS by SnO_2 NPs under light is due to their photocatalytic activity, which involves the creation of electron−hole pairs and subsequent reactions with water or oxygen molecules in the surrounding environment. The mechanism of ROS formation is likely mediated by the transfer of electrons from the conduction band of SnO_2 to absorb oxygen molecules on the surface of the NPs.[2,16]

2.2. UV−Vis Absorption Spectrum. UV−visible spectroscopy may be used to figure out the optical band gap of semiconductors;[17] therefore, UV−visible absorption spectra of SnO_2 NPs were carried out from 200 to 1100 nm, as shown in Figure 3A. The absorption edge of semiconductor NPs moves to a higher energy as the particle size declines, and the quantum confinement effect is expected to increase. The wavelength cut of SnO_2 NPs was reported to be 205 nm, as seen in the absorption spectra in Figure 3A.

2.3. Fourier Transform Infrared Spectroscopy. To look for possible biomolecules on the surface of NPs, the reaction mixture was evaluated with Fourier transform infrared (FTIR) measurements. There were four different peaks in the spectra at the wavelengths of 3297.75, 2102.02, 1638.12, and 1021.46 cm^{-1}, as shown in Figure 3B. The peak at 3297.75 cm^{-1}, distinguished by the hydrogen bonding group of OH, aids in the stretching vibration of alcohol phenols, could be caused by the inception of NPs from the aqueous phase, while the peak at 2102.022 cm^{-1} could be caused by the stretch of the C−H bond of the methylene groups of protein and the N−H stretch of the amine salt.[18] The above result is most likely owing to the electrical environment of the methylene groups being intimidated by vicinal carbonyl plus SnO_2 NPs. C═O stretching of amino acid residues is measured at 1638.12 cm^{-1},[19] whereas C−O stretching of alcohols, esters, and carboxylic acids plus C−N stretching of aliphatic amines is recorded at 1021.46 cm^{-1}.[20] We may extrapolate from these observations that the protein in the supernatant acts as a stabilizing capping factor and can connect to SnO_2 NPs via unbound cysteine or amine groups in proteins.

2.4. X-ray Diffraction and Energy-Dispersive X-ray Spectroscopy Analyses. The crystalline structure of produced SnO_2 NPs is shown by the X-ray diffraction (XRD) pattern exhibited in Figure 4A. Significant peaks in the 2θ range of 10−80° were detected at 25.38, 37.97, 48.14, 54.40, and 62.71°, respectively, which fit well with the Miller index (*hkl*) values of (101), (004), (200), (105), and (204), supporting the anatase phase. Furthermore, a weak peak was also discovered at 30.98°, which was attributed to the

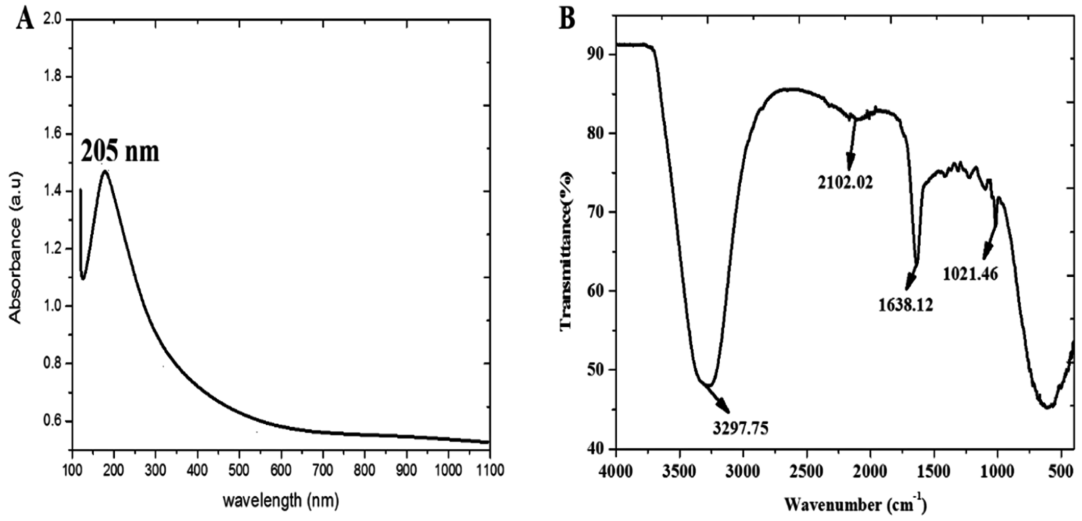

Figure 3. (A) UV spectroscopic and (B) formal FTIR analysis of *E. hormaechei*-mediated SnO_2 NPs. The UV and FTIR spectrums of *E. hormaechei* and pure SnO_2 are also shown in supplementary Figures 1 and 2, respectively.

https://doi.org/10.1021/acsomega.3c02932
ACS Omega 2023, 8, 27439−27449

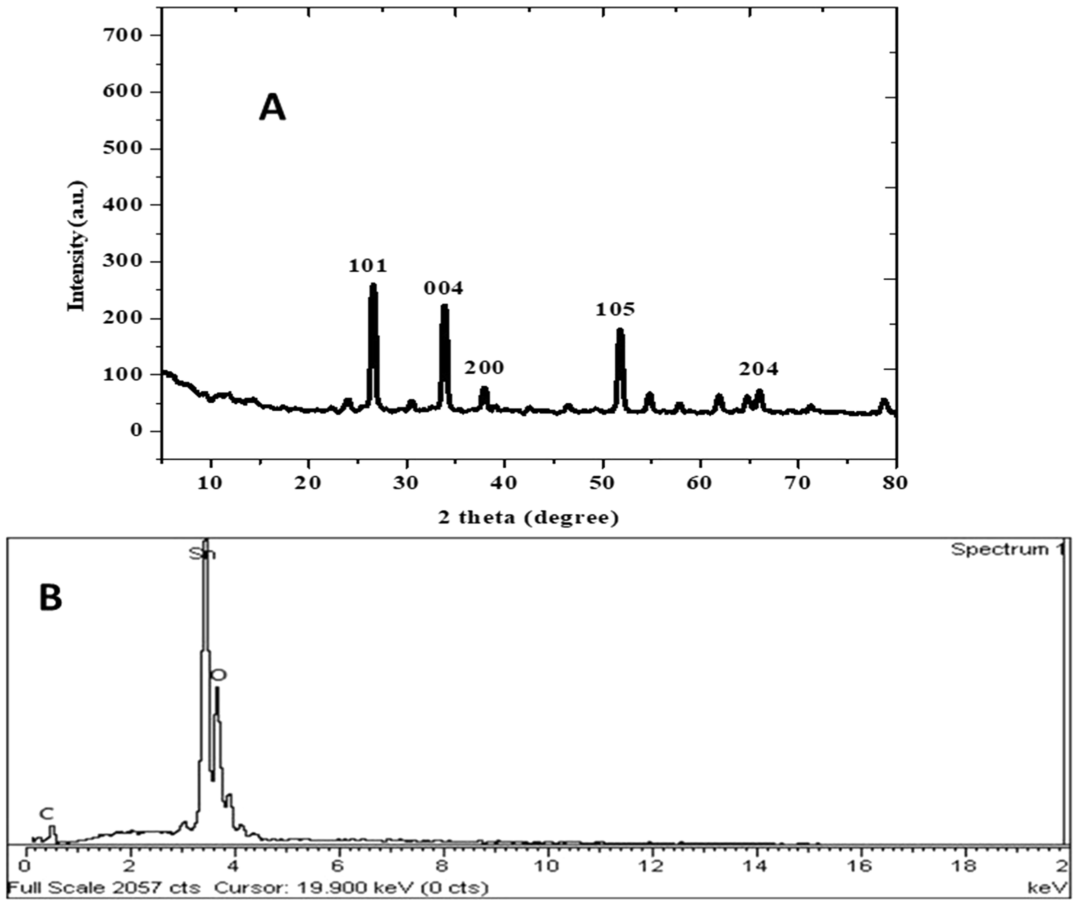

Figure 4. (A) XRD graphical representation and (B) EDX elemental analysis of *E. hormaechei* strain-mediated SnO_2 NPs.

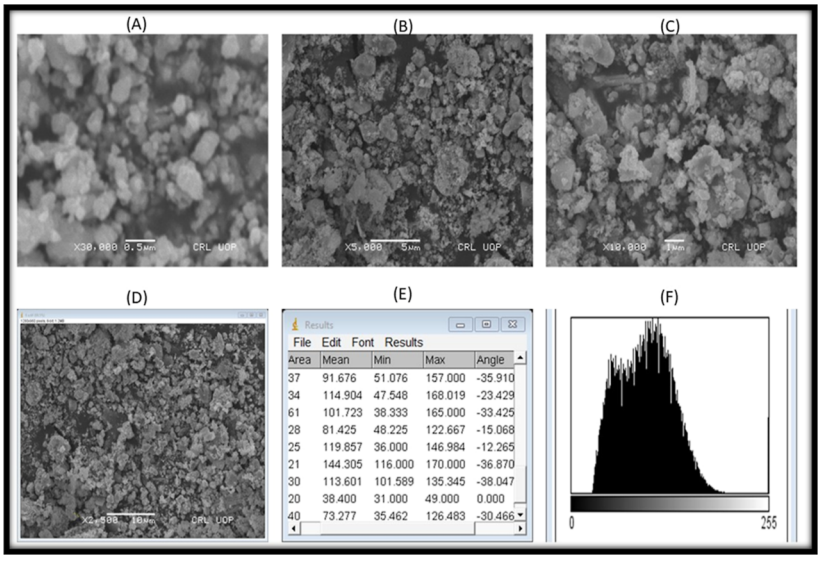

Figure 5. SEM micrographs; (A) 500 nm scale bar, (B) 1 μm scale bar, (C) 5 μm scale bar, (D) 10 μm scale bar, (E) image analysis results of micrographs, and (F) size distribution graph.

orthorhombic crystalline structure. The outcomes were validated using JCPDS (Joint Committee on Powder Diffraction Standards) card no. 78-2486. The crystalline size of the particles was enumerated using the Debye Scherrer's equation ($d = 0.89l/b \cos 4$), where d is the NPs' crystalline size, w is the X-ray radiation source's wavelength, 0.89 is a constant crystalline form factor, and d is the Bragg's diffraction angle, while the full angular width at half maximum of XRD peaks was recorded at diffraction angle 2.[21] The average crystalline size of green synthesized SnO_2 NPs was determined to be 10 nm. The energy-dispersive X-ray spectroscopy (EDX) spectra of produced SnO_2 NPs are illustrated in Figure 4B. The EDX spectrum confirms that all produced SnO_2 NPs contain solely Sn and that the purity of the SnO_2 NPs is very high.[22]

https://doi.org/10.1021/acsomega.3c02932
ACS Omega 2023, 8, 27439−27449

2.5. Scanning Electron Microscopy. The morphological characteristics of synthesized NPs were investigated through scanning electron microscopy (SEM). SEM analysis helps to scrutinize the surface shape and chemical content of the produced SnO_2 NPs, as depicted in Figure 5. The typical size of SnO_2 NPs was found to be approximately 12 nm or less, as seen in the micrograph in Figure 5. Furthermore, the shape of the SnO_2 NPs was discovered to be spherical in this investigation.[23]

2.6. Antibacterial Assay of SnO_2 NPs against Sinusitis Pathogens. The antibacterial potential of SnO_2 NPs was tested against four distinct sinusitis pathogens, namely *Haemophilus influenza*, *Streptococcus pyogenes*, *Moraxella catarrhalis*, and *Streptococcus pneumoniae*. The generation of reactive oxygen species (ROS) with light exposure, the breakdown of metal oxide NPs, and the electrostatic correspondence of NPs with microbial cell walls have all been postulated as modes of action for metal oxide NPs against bacteria.[24] The aggregation of SnO_2 NPs mostly on the exterior of the bacterial membrane could be a reason for their antibacterial activity. SnO_2 NPs create ROS, which consort with the bacterial membrane, causing membrane permeability and cell death.[25,26] The bacterial death is proposed to be induced by the release of Sn^{4+} from SnO_2 NPs under light. This involves photoinduced electron transfer from the conduction band of SnO_2 NPs to adsorbed O_2 molecules, resulting in the formation of superoxide anions (O_2-) and holes in the valence band of SnO_2. These holes can react with surface-adsorbed water molecules to form hydroxyl radicals ($^{\bullet}OH$), which can oxidize SnO_2 and lead to the release of Sn^{4+} ions. The released Sn^{4+} ions can potentially interact with bacterial cells, leading to damage of bacterial mitochondria and DNA, as seen in Figure 6.[27] The results of the disc diffusion

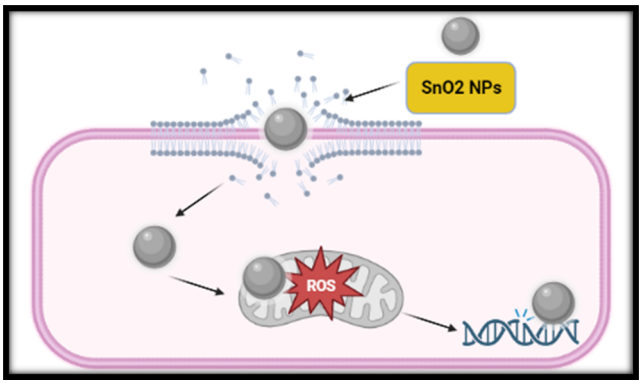

Figure 6. Mechanistic approach of SnO_2 NPs for inducing cytotoxicity in bacterial cells.

test, minimal inhibitory concentration (MIC), and minimum bactericidal concentration (MBC) of SnO_2 NPs are represented in Table 1. For the disc diffusion test, the highest value was observed for *S. pyogenes* (19.75 ± 0.46), followed by *M. catarrhalis* (17.49 ± 0.82) and *Haemophilus influenzae* (15.31 ± 0.73), respectively. The appearance of a clear zone around the SnO_2 NP disc, demonstrated that the SnO_2 NPs had antibacterial activity, inhibiting the growth of the sinusitis pathogens. In this study, the disc diffusion test was defined as a preliminary inquiry for assessing the antibacterial activity. As a result, a more detailed evaluation of SnO_2 NPs' antibacterial activity using the MIC value was necessary. The MIC was

Table 1. Antibacterial Potential of SnO_2 NPs against Sinusitis Pathogens

bacterial strains	zone of inhibition (mm)	MIC (mg/mL)	MBC (mg/mL)
M. catarrhalis	17.49 ± 0.82	5.6	6.2
S. pneumoniae	12.16 ± 0.25	6.3	7.1
S. pyogenes	19.75 ± 0.46	4.2	4.8
H. influenzae	15.31 ± 0.73	3.4	3.6

calculated by serial dilution as the smallest amount of antimicrobials necessary to impede bacterial multiplication, as indicated in Table 1. The MIC values of SnO_2 NPs against sinusitis pathogens ranged from 3.4 to 6.3 mg/mL. *S. pneumoniae*, *M. catarrhalis*, *S. pyogenes*, and *H. influenzae* had MIC values of 6.3, 5.6, 4.2, and 3.4 mg/mL, respectively. The investigation found MBC values of 7.1, 6.2, 4.8, and 3.6 mg/mL for *S. pneumoniae*, *M. catarrhalis*, *S. pyogenes*, and *H. influenzae*, respectively. Our results support the previously published literature in which NPs have been reported to be active against *S. pyogenes*,[28] *M. catarrhalis*,[29] and *H. influenzae*.[30]

2.7. Anti-larvicidal Activity. Dengue fever has become much more common in recent decades worldwide. Combating disease-carrying mosquitoes is the most effective way to control the spread of the dengue virus. Material scientists have recently been increasingly focused on finding superior alternatives in plant extracts and bacterium-assisted NPs against the proposed vector as the mechanistic approach of using NPs to fight mosquito-based diseases. A variety of concentrations of synthesized SnO_2 NPs (25, 50, 100, 150, and 200 ppm) were evaluated against *Aedes aegypti* second and fourth instars in this assay. At 200 ppm, the highest percent mortality of 63.6 ± 0.81 was found, followed by 22.4 ± 0.19% at 25 ppm. Mortality decreases in lockstep with lower doses, as shown in Table 2. Our study is also in line with previously published data, where green synthesized silver NPs were found to be active against dengue larvae in a dose-dependent manner.[31]

2.8. Anti-inflammatory Assay. Inflammation is a localized, vascularized, or inflammatory response to poisons and irritants. Natural products' anti-inflammatory properties are based on their traditional uses.[32] Natural products produced by plants and microbes are an important class of plant secondary metabolites that can block key enzymes involved in the inflammatory cycle, giving them anti-inflammatory effects.[33] Cyclooxygenase (COX-1 and COX-2) and lipoxygenase (15LOX) are key players for inflammation and are used as pharmacological targets. Whereas phospholipase (sPLA) is a key inflammatory mediator, and its inhibition also leads to the reduction of inflammation. Inhibition of the COX-1 and COX-2 and LOX pathways by SnO_2 NPs results in significant anti-inflammatory effects, as represented in Figure 7A,B.[34] Secondary metabolites are a type of bacterial molecules that can decrease key enzymes involved in the inflammatory cycle, implying that SnO_2 NPs have anti-inflammatory capabilities[35] Leukotrienes and prostanoids are reduced when COX-1 and COX-2, sPLA2, and 15-LOX—the enzymes that generate eicosanoids—are inhibited. Among the used concentrations, the highest inhibition of 76.8 ± 0.93 was observed at 400 μg/m for 15-LOX, followed by 67.4 ± 0.91 for COX-1, respectively. SnO_2 NPs have been demonstrated to have improved anti-inflammatory efficacy in these investigations, as

https://doi.org/10.1021/acsomega.3c02932
ACS Omega 2023, 8, 27439−27449

Table 2. Anti-larvicidal Potential of Synthesized SnO_2 NPs

	concentrations in PPM				
	25	50	100	150	200
mortality %	22.4 ± 0.19	36.09 ± 0.49	44 ± 0.37	57 ± 0.57	63.6 ± 0.81

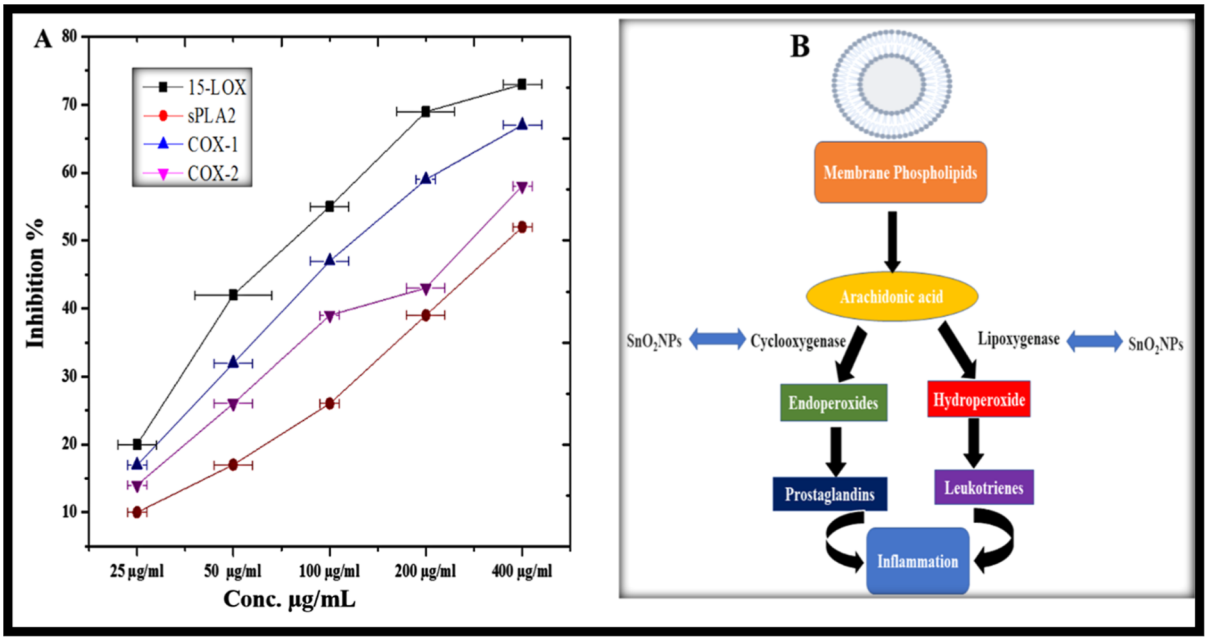

Figure 7. (A) Anti-inflammatory effect of synthesized SnO_2 NPs, (B) mechanistic approach to how arachidonic acid produces and inhibits inflammatory responses.

Table 3. AchE and BchE Inhibitory Responses of Synthesized SnO_2 NPs

	concentrations in µg/mL				
	62.5	125	250	500	1000
AchE	22.14 ± 0.75	39.09 ± 0.49	58.42 ± 0.37	66.61 ± 0.57	77.54 ± 0.26
BchE	19.32 ± 0.86	31 ± 0.43	52.74 ± 0.52	52.92 ± 0.48	68.36 ± 0.47

they were found to suppress the enzymes that induce inflammation. Same results were seen in another research work when the green synthesized silver NPs were tested for anti-inflammatory activity.[36]

2.9. In Vitro Anti-Alzheimer's Efficacy of SnO_2 NPs. Alzheimer's disease (AD) is a neurological illness that accounts for 60−80% of dementia cases globally. Memory, executive and visual spatial skills, personality, and language are all affected by this condition. The illness's prevalence rate is worrying, with one person developing Alzheimer's disease every 65 s in the United States alone. Cholinesterase inhibitors are currently accessible for people with any stage of Alzheimer's disease. The efficient suppression of cholinesterase enzymes has been documented using a variety of synthetic and natural compounds.[37] The NPs capped with bacterial natural products could block the active sites of enzymes and thus prevent substrate binding. The current study investigated the inhibitory potential of SnO_2 NPs against two cholinesterase enzymes, acetylcholinesterase (AchE) and butyrylcholinesterase (BchE), at doses ranging from 62.5 to 1000 µg/mL, as shown in Table 3. The NPs' inhibitory responses of SnO_2 NPs against both the enzymes were revealed to be dose-dependent. At 1000 µg/mL, the NPs were extremely active, inhibiting AchE by 77.54 ± 0.26% and BchE by 68.36 ± 0.47%. At 62.5 µg/mL, the percent inhibition response of SnO_2 NPs against AchE had a value of 22.14 ± 0.75, whereas BchE had a value of 19.32 ± 0.86, respectively. Overall, the particles were very active against both cholinesterase enzymes, as evidenced by their large IC_{50} values of 176 g/mL for AchE and 168 µg/mL for BchE, respectively. The same in vitro assays have been used previously to show the anti-Alzheimer's activity of prospective drugs.[38−40] Therefore, based on the results of these assays, it is proposed that the SnO_2 NPs have the potential to be exploited for the targeted administration of prospective Alzheimer's treatments. However, more research is needed to improve biocompatibility and study SnO_2 NPs' in vivo toxicity.

2.10. Anti-aging Assay. In this research work, the anti-aging efficacy of the *E. hormaechei* extract-mediated SnO_2 NPs was also tested. The test samples were evaluated in vitro for their ability to inhibit enzymes such as tyrosinase, elastase, collagenase, hyaluronidase, and advanced glycation end (AGE) products at a given concentration. Extracellular matrix components in the dermis are degraded by enzymes such as collagenase, hyaluronidase, and elastase. Deep wrinkles, skin tonus, and skin resilience losses are all caused by these enzymes.[41−43] Tyrosinase deficiency causes aging and is the primary cause of malignant melanoma, freckles, and Melissa-like pigmentary diseases. According to the research, oxidative

https://doi.org/10.1021/acsomega.3c02932
ACS Omega 2023, 8, 27439−27449

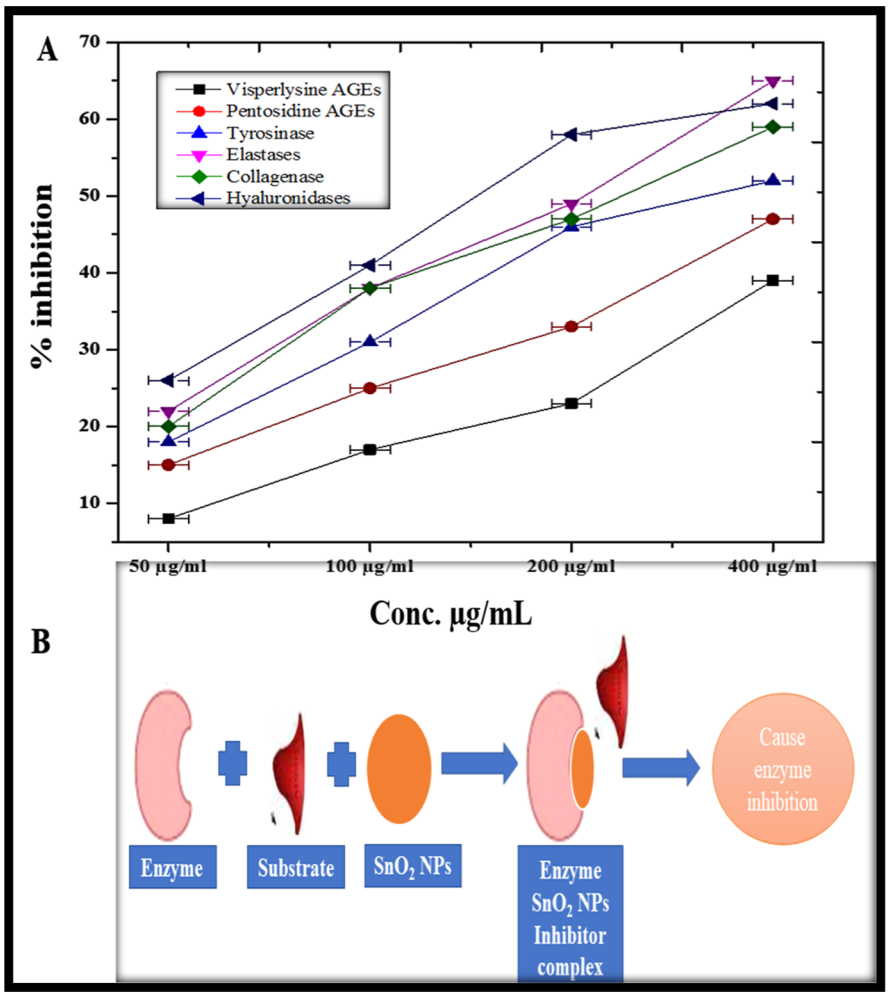

Figure 8. (A) Anti-aging findings of synthesized NPs at different concentrations, (B) mechanistic approach to how NPs inhibit enzyme activity.

stress causes advanced glycation and generates end products termed as advanced glycation end products (AGEs). These AGEs are linked to aging and age-related disorders.[44,45] NPs have been shown to have considerable inhibitory effects on elastase (65.4 ± 0.72), followed by visperlysine AGEs (39.6 ± 0.21) and (59.3 ± 0.64) against collagenase. The whole anti-aging potential at different concentrations is detailed in Figure 8.

3. CONCLUSIONS

In summary, the current study revealed that metallic tin oxide NPs (SnO_2 NPs) could be generated successfully using the *E. hormaechei* EAF63 strain. The biomass of *E. hormaechei* contains proteins, carbohydrates, and lipid chemicals, which could help in the capping and reduction of NPs. SnO_2 NPs showed potential therapeutic effects in different biomedical applications. Enhanced antimicrobial and anti-larvicidial activity of SnO_2 NPs was observed, which indicates their potential against sinusitis pathogens and *A. aegypti,* respectively. Similarly, SnO_2NPs showed better efficiency against anti-aging enzymes. Furthermore, significant inhibitory effectiveness against lipoxygenase (15-LOX), phospholipase (sPLA2), cyclooxygenase (COX-1 and COX-2), AchE, and BchE was also estimated, showing a positive sign in the discovery of therapeutics for inflammation and Alzheimer's-like deadly diseases. Therefore, it is concluded that the *E. hormaechei* strain EAF63-mediated SnO_2 NPs exhibit potential to be used as an effective nanoplatform conducive to an array of biomedical applications in the near future. Nevertheless, it is also suggested to conduct further studies, particularly in in vivo models, to increase the biocompatibility of SnO_2 NPs.

4. METHODS

4.1. Biosynthesis of SnO_2 NPs Using *E. hormaechei* Strain EAF63. SnO_2 NPs were generated using a previously described method with few new modifications.[9,46] *E. hormaechei* EAF63 was isolated from the hospital road side and identified (Gene bank accession number JF783991.1). *E. hormaechei* was inoculated in nutrient broth (NB) and incubated for 24 h before being diluted four times with fresh NB to a final volume of 100 mL and incubated for another 24 h. Using the bacterial synthesis method of NPs, *E. hormaechei* strain was used to reduce and stabilize Sn^{2+} ions. In a 100 mL Erlenmeyer flask, reaction mixtures were prepared by mixing 20 mL of biomass with 100 mL of 1 mM stannous chloride solution at ambient temperature. The solutions were stirred constantly at 60−70 °C for 8 h before being stirred again at 37 °C for 24 h. At 14,000 rpm for 10 min, multiple centrifugations were used to purify SnO_2 NPs and then dried at 80 °C. The dried powder was carefully collected and preserved for further characterization and biological investigation[47]

https://doi.org/10.1021/acsomega.3c02932
ACS Omega 2023, 8, 27439−27449

4.2. Characterization of Biogenic SnO_2 NPs. Advanced tools were used to assess the physicochemical and morphological features of biosynthesized SnO_2 NPs.[48] UV spectroscopy uses the typical range of 200−1100 nm to monitor the interaction between biomass and metallic salt. The crystal nature of biologically synthesized SnO_2 NPs was evaluated through the XRD profile. Panalytical's X'Pert X-ray diffractometer was utilized to produce the XRD peaks at Cu Kα (= 1.54056 Å). SnO_2 NPs were studied using FTIR spectroscopy in the 400−4000 cm^{-1} spectrum region to reveal and assess related functional groups involved in their biosynthesis approach.[49] SEM was applied to measure the physical dimensions and morphological characteristics of biosynthesized SnO_2 NPs (JSM-5910, Japan). EDX spectroscopy was used to verify the primary formulation of the biogenic SnO_2 NPs.[50]

4.3. Antibacterial Activity. *4.3.1. Bacterial Strain Preparation.* The Khyber Teaching Hospital provided us with *H. influenza*, *S. pyogenes*, *M. catarrhalis,* and *Streptococcus pneumonia* for antibacterial assays. All of the bacterial strains were grown for 24 h at 37 °C with 200 rpm agitation in Mueller Hinton broth (MHB) (Merck, Germany). SnO_2 NPs were dissolved in dimethyl sulfoxide (DMSO) to all in vitro biochemical assays.

4.3.2. Utilizing the Disc Diffusion Experiment to Test for Antimicrobial Susceptibility. Resazurin solution was made at a concentration of 0.02% (w/v) by using the following protocol. In 10 mL of distilled water, 0.002 g of resazurin salt powder was disintegrated and vortexed. Millipore membrane filters were used to filter the mixture (0.2 mm). For analyzing the antimicrobial potential of biogenic SnO_2 NPs, the Kirby−Bauer disk diffusion susceptibility technique was utilized.

4.3.3. Determination of MIC and MBC. The MIC and MBC of biogenic SnO_2 NPs were determined with the help of CLSI guideline techniques. The MIC test was carried out using normal broth micro dilution procedures using a 96-well microtiter plate with a round bottom, while Mueller Hinton Agar (MHA) plates were used for the MBC assessment. The bacteria were inoculated at a concentration of 10^6 cfu/mL. 100 mL of synthesized SnO_2 NP stock solution (500 mg/mL) was added to 100 mL of MHB for the MIC test; the bacterial inoculums were subjected to a two time dilution with the bacterial inoculums from column 12 to column 3. The largest concentration of SnO_2 NPs was found in column 12 of the microtiter plate, while the lowest concentration was found in column 3. The negative control (just medium) was in column 1, while the positive control was in column 2 (medium and bacterial inoculums). 30 mL of resazurin solution was applied into respective wells and left to incubate for 24 h at 37 °C. After incubation, color shifts were noticed. No bacterial growth was indicated by the blue/purple tint, while bacterial growth was indicated by the pink/colorless color. The MIC value was calculated using the smallest concentration of antimicrobials that prevent bacteria from growing. The MBC is the smallest concentration of antimicrobials required to totally kill bacteria. For the MBC assay, each microtiter plate well's suspension was deposited onto MHA plates. The plates were incubated for 24 h at 37 °C. The MBC value was calculated using the smallest amount with no apparent bacterial growth over the MHA plate.[51,52]

4.4. Anti-larvicidal Activity. SnO_2 NPs were studied to demonstrate their anti-larvicidal activity against the larvae of the dengue vector, *A. aegypti* L. The previously used standard procedure was applied with minimal modifications.[53] Five groups were employed, four of which included 25 third instar larvae each (for varying concentrations) and one of which served as a control group. In a sterile well plate, each well contained 25 third instar larvae in 200 mL of the SnO_2 NP solution at the appropriate concentration and distilled water as a negative control. The well plate was incubated under conventional insectary settings, which included a 12 h light to 12 h dark photoperiod, with a relative humidity of 80% on average and a temp of 28 °C. The larvae were not fed during the trials. After 24 h, the percentage of those who died was analyzed. Those specimens that could not move or moved sluggishly in response to tactile stimulation were counted as dead. The experiment was repeated five times, with the percent mortality representing the average of the five triplicates.

4.5. Anti-inflammatory Activities. *4.5.1. Inhibitory Performance against COX-1 and COX-2.* The inhibitory potential of COX-1 (Ovine kit 701,050 France) and COX-2 (Human kit 701,050 France) for testing materials was assessed. Ibuprofen (10 M) was employed as a positive control, whereas arachidonic acid (1.1 mM) was utilized as a reagent. Both COXs were recorded according to the equipment's manufacturer's specifications. In a 96-well plate, the test was performed in triplicate. A Synergy II reader was applied to measure *N*,*N*,*N*-,*N*-tetramethyl-*p*-phenylenediamine at 590 nm in a 96-well microplate.[54]

4.5.2. Inhibitory Performance against 15-LOX. SnO_2 NPs were assessed in order to evaluate their inhibitory performance against 15-LOX (760,700 kit, Cayman, France). 100 μM nordihydroguaiaretic acid (NDGA) was considered as the positive control. Both positive and negative controls were prepared with 10 μM arachidonic acid. Using the soy 15-lipooxygenase standard, the amount of hydroperoxides generated by the lipooxygenation mechanism in 10 mM Tris−HCl buffer at a 7.4 pH filter included in the kit was determined. The SnO_2 NPs and enzymes were loaded in a 96-well plate and incubated for 5 min before recording the absorbance at 940 nm with a Synergy II reader (BioTek Instruments, Colmar, France). The inhibitor was added to the enzyme cocktail following 5 min of incubation. The substrate was introduced to the pre-incubated sample following 5 min of incubation, accompanied by the chromogen, and then the absorbance was measured.[55]

4.5.3. Inhibitory Performance against Secretory Phospholipase A2. The inhibitory potential of SnO_2 NPs was assessed against sPLA2, using an assay kit (10,004,883, Cayman Chem. Co, Montluçon, France). 4 mmol diheptanoyl thio-PC and 100 mmol thiotheramide-PC were taken as standard controls. The diheptanoylthio-PC ester is cleaved, releasing free thiols, which were identified using 5,5′-dithio-bis-(2-nitrobenzoic acid) (DTNB) at 420 nm in a 96-well microplate.

4.6. Anti-Alzheimer's Assay. The capacity of SnO_2 NPs to impede AchE and BchE was checked at different concentrations that range from 62 to 1000 μg/mL using a previously established protocol.[55,56] Phosphate-buffered saline, 5, 5-dithiobisnitrobenzoic acid, acetylcholine iodide, and butyrylcholine iodide were used to make the substrate solution. As a positive control, the pristine reaction mixture was used, while galantamine hydrobromide (5 mg/0.5 mL methanol) was employed as a negative control. Finally, the absorbance of test samples at 412 nm was determined. The inhibitory activities of enzymes were determined using the following formula: percentage inhibition (%) = 100 − enzyme activity

https://doi.org/10.1021/acsomega.3c02932
ACS Omega 2023, 8, 27439−27449

(%), where enzyme activity (%) = $(V/V_{max}) \times 100$. In this equation, V is defined as the rate of absorption with change in time ($V = \Delta Abs/\Delta t$) and V_{max} is the activity of enzyme without the presence of drugs.

4.7. Anti-aging Assay. *4.7.1. Anti-AGE Formation Activity.* The inhibitory ability of SnO_2 NPs against the production of vesperlysine AGEs and pentosidine AGEs was determined using the previous protocol.[54] For this purpose, 0.5 M glucose and 0.1 M phosphate buffer (pH 7.4) containing 0.02% (w/v) sodium azide were used to make bovine serum albumin (BSA) solution. The test samples were combined with a 20 mg/mL BSA solution. At 37 °C, the reaction mixture was kept in the dark for 5 days. The quantity of fluorescence generated had been determined with a Bio-Rad VersaFluor fluorometer at Marnes-la-Coquette, France, by measuring absorbance at a 330 nm excitation wavelength and a 410 nm emission wavelength, respectively.

4.7.2. Tyrosinase Assay. The tyrosinase test was performed using the previously reported technique of,[57] which employed L-DOPA (5 mM; Sigma-Aldrich). The test sample was combined with 10 L of the L-DOPA diphenolase substrate and sodium phosphate buffer (50 mM, pH 6.8). By adding 0.2 mg/mL of mushroom tyrosinase solution to the reaction mixture, the final volume was increased to 200 L (Sigma-Aldrich). As a control, the DMSO solvent was utilized to replace the tested sample. At 475 nm, the reaction activities were monitored using a microplate reader (BioTek ELX800; BioTek Instruments). Percent inhibition was calculated in comparison to the matching control tyrosinase effect.

4.7.3. Elastase Assay. The inhibition of elastase in porcine pancreatic elastase was studied (Sigma-Aldrich). In this experiment, the substrate was *N*-Succ-Ala-Ala-Ala-*p*-nitroanilide. The reaction's optical density (OD) was determined using a microplate reader (BioTek ELX800; BioTek Instruments) based on the relative conversion of the substrate to nitroaniline at a wavelength of 410 nm.[57] The anti-elastase potential was measured three times and represented as % inhibition compared to the relevant power.

4.7.4. Hyaluronidase Assay. Methodology devised by ref 57 was employed to measure the hyaluronidase inhibitory potential of test substances. As a substrate, 0.03% (w/v) hyaluronic acid solution with 1.5 units of hyaluronidase (Sigma-Aldrich) was utilized. An acid albumin solution (0.1% w/v BSA) was used to precipitate the undigested form of hyaluronic acid. A microplate reader was used to determine the OD at a 600 nm wavelength (BioTek ELX800; BioTek Instruments, Colmar, France). The anti-hyaluronidase potential was represented as a percentage inhibition, unlike with the corresponding control.

4.7.5. Collagenase Assay. The collagenase inhibitory experiment was carried out using a modified version of a procedure described in ref 57. The substrate in this experiment was [(2-furyl) acryloyl]-Leu-Gly-Pro-Ala (FALGPA; Sigma-Aldrich). Using a microplate reader with an OD of 335 nm, the decline in FALGPA absorption was monitored for 20 min (BioTek ELX800; BioTek Instruments, Colmar, France). In contrast to the control anti-collagenase, the experiment was performed three times, and the % inhibition was measured after each repetition.

AUTHOR INFORMATION

Corresponding Authors

Muhammad Rizwan − *Center for Biotechnology and Microbiology, University of Swat, Swat 19120 Khyber Pakhtunkhwa, Pakistan*; Email: muhammad.rizwan@uswat.edu.pk

Shah Faisal − *Institute of Biotechnology and Microbiology, Bacha Khan University, Charsadda 24460 Khyber Pakhtunkhwa, Pakistan*; orcid.org/0000-0001-5474-2622; Email: Shahfaisal11495@gmail.com

Authors

Muhammad Hamza Tariq − *Institute of Biological Chemistry, Academia Sinica, Taipei 115, Taiwan*

Sania Zafar − *Institute of Molecular Biology and Biotechnology, Bahauddin Zakariya University, Multan 60000, Pakistan*

Ajmal Khan − *Institute of Biotechnology and Microbiology, Bacha Khan University, Charsadda 24460 Khyber Pakhtunkhwa, Pakistan*

Farhan Ahmad − *Institute of Biotechnology and Microbiology, Bacha Khan University, Charsadda 24460 Khyber Pakhtunkhwa, Pakistan*

Complete contact information is available at: https://pubs.acs.org/10.1021/acsomega.3c02932

Funding

No fund was taken from any source.

Notes

The authors declare no competing financial interest.

The ethical approval for the current study was taken from the Center for Biotechnology and Microbiology, University of Swat, KPK, Pakistan.

ACKNOWLEDGMENTS

We are grateful to the Center for Biotechnology and Microbiology, University of Swat, KPK, Pakistan, for providing us research facilities.

REFERENCES

(1) Dorgham, R. A.; Abd Al Moaty, M. N.; Chong, K. P.; Elwakil, B. H. Molasses-Silver Nanoparticles: Synthesis, Optimization, Characterization, and Antibiofilm Activity. *Int. J. Mol. Sci.* **2022**, *23*, 10243.

(2) Li, Y.; Xia, Y.; Liu, K.; Ye, K.; Wang, Q.; Zhang, S.; Huang, Y.; Liu, H. Constructing Fe-MOF-derived Z-scheme photocatalysts with enhanced charge transport: nanointerface and carbon sheath synergistic effect. *ACS Appl. Mater. Interfaces* **2020**, *12*, 25494−25502.

(3) El-Attar, A. A.; El-Wakil, H. B.; Hassanin, A. H.; Bakr, B. A.; Almutairi, T. M.; Hagar, M.; Elwakil, B. H.; Olama, Z. A. Silver/Snail Mucous PVA Nanofibers: Electrospun Synthesis and Antibacterial and Wound Healing Activities. *Membr* **2022**, *12*, 536.

(4) Ridolfo, R.; Tavakoli, S.; Junnuthula, V.; Williams, D. S.; Urtti, A.; van Hest, J. C. Exploring the impact of morphology on the properties of biodegradable nanoparticles and their diffusion in complex biological medium. *Biomacromolecules* **2020**, *22*, 126−133.

(5) Aljohani, F. S.; Hamed, M. T.; Bakr, B. A.; Shahin, Y. H.; Abu-Serie, M. M.; Awaad, A. K.; El-Kady, H.; Elwakil, B. H. In vivo biodistribution and acute toxicity evaluation of greenly synthesized ultrasmall gold nanoparticles with different biological activities. *Sci. Rep.* **2022**, *12*, 6269.

(6) Qin, T.; Wang, Z.; Wang, Y.; Besenbacher, F.; Otyepka, M.; Dong, M. Recent progress in emerging two-dimensional transition metal carbides. *Nano-Micro Lett.* **2021**, *13*, 183.

(7) Sagadevan, S.; Lett, J. A.; Fatimah, I.; Lokanathan, Y.; Léonard, E.; Oh, W. C.; Hossain, M. A. M.; Johan, M. R. Current trends in the green syntheses of tin oxide nanoparticles and their biomedical applications. *Mater. Res. Express* **2021**, *8*, 082001.
(8) Shanmuganathan, R.; Karuppusamy, I.; Saravanan, M.; Muthukumar, H.; Ponnuchamy, K.; Ramkumar, V. S.; Pugazhendhi, A. Synthesis of silver nanoparticles and their biomedical applications-a comprehensive review. *Curr. Pharm. Des.* **2019**, *25*, 2650−2660.
(9) Tsekhmistrenko, S. I.; Bityutskyy, V. S.; Tsekhmistrenko, O. S.; Horalskyi, L. P.; Tymoshok, N. O.; Spivak, M. Y. Bacterial synthesis of nanoparticles: A green approach. *Biosyst. Divers.* **2020**, *28*, 9−17.
(10) Batool, M.; Khurshid, S.; Qureshi, Z.; Hassan, A.; Siddique, M. B. A.; Naveed, S.; Siddique, S. A. Study of biogenically fabricated transition metal oxides nanoparticles on oral cavity infectious microbial strains. *Inorg. Nano-Met. Chem.* **2021**, *51*, 856−866.
(11) Irshad, M. A.; Nawaz, R.; Rehman, M. Z. U.; Adrees, M.; Rizwan, M.; Ali, S.; Ahmad, S.; Tasleem, S. Synthesis, characterization and advanced sustainable applications of titanium dioxide nanoparticles: A review. *Ecotoxicol. Environ. Saf.* **2021**, *212*, 111978.
(12) Mohd Yusof, H.; Mohamad, R.; Zaidan, U. H.; Abdul Rahman, N. A. Microbial synthesis of zinc oxide nanoparticles and their potential application as an antimicrobial agent and a feed supplement in animal industry: a review. *J. Anim. Sci. Biotechnol.* **2019**, *10*, 57.
(13) Zikalala, N.; Matshetshe, K.; Parani, S.; Oluwafemi, O. S. Biosynthesis protocols for colloidal metal oxide nanoparticles. *Nano-Struct. Nano-Objects* **2018**, *16*, 288−299.
(14) Gebreslassie, Y. T.; Gebretnsae, H. G. Green and cost-effective synthesis of tin oxide nanoparticles: a review on the synthesis methodologies, mechanism of formation, and their potential applications. *Nanoscale Res. Lett.* **2021**, *16*, 97.
(15) Nadeem, M.; Tungmunnithum, D.; Hano, C.; Abbasi, B. H.; Hashmi, S. S.; Ahmad, W.; Zahir, A. The current trends in the green syntheses of titanium oxide nanoparticles and their applications. *Green Chem. Lett. Rev.* **2018**, *11*, 492−502.
(16) Tan, C.; Tao, R.; Yang, Z.; Yang, L.; Huang, X.; Yang, Y.; Qi, F.; Wang, Z. Tune the photoresponse of monolayer MoS2 by decorating CsPbBr3 perovskite nanoparticles. *Chin. Chem. Lett.* **2023**, *34*, 107979.
(17) Ahmad, W.; Jaiswal, K. K.; Soni, S. Green synthesis of titanium dioxide (TiO2) nanoparticles by using Mentha arvensis leaves extract and its antimicrobial properties. *Inorg. Nano-Met. Chem.* **2020**, *50*, 1032−1038.
(18) Olajire, A.; Mohammed, A. Green synthesis of palladium nanoparticles using Ananas comosus leaf extract for solid-phase photocatalytic degradation of low density polyethylene film. *J. Environ. Chem. Eng.* **2019**, *7*, 103270.
(19) Jabbar, A. H.; Al-janabi, H. S. O.; Hamzah, M. Q.; Mezan, S. O.; Tumah, A. N.; Ameruddin, A. S. B.; Agam, M. A. Green synthesis and characterization of silver nanoparticle (AgNPs) using pandanus atrocarpus extract. *Int. J. Adv. Sci. Technol.* **2020**, *29*, 4913−4922.
(20) Amaliyah, S.; Masruri, M.; Sabarudin, A.; Sumitro, S. B. Sonication-assisted green synthesis of silver nanoparticles using Piper retrofractum fruit extract and their antimicrobial assay. *AIP Conf. Proc.* **2021**, *2349*, 020003.
(21) Parthibavarman, M.; Sathishkumar, S.; Prabhakaran, S. Enhanced visible light photocatalytic activity of tin oxide nanoparticles synthesized by different microwave optimum conditions. *J. Mater. Sci.: Mater. Electron.* **2018**, *29*, 2341−2350.
(22) Srinivasan, M.; Venkatesan, M.; Arumugam, V.; Natesan, G.; Saravanan, N.; Murugesan, S.; Ramachandran, S.; Ayyasamy, R.; Pugazhendhi, A. Green synthesis and characterization of titanium dioxide nanoparticles (TiO2 NPs) using Sesbania grandiflora and evaluation of toxicity in zebrafish embryos. *Process Biochem.* **2019**, *80*, 197−202.
(23) Rao, T. N.; Riyazuddin; Babji, P.; Ahmad, N.; Khan, R. A.; Hassan, I.; Shahzad, S. A.; Husain, F. M. Green synthesis, and structural classification of Acacia nilotica mediated-silver doped titanium oxide (Ag/TiO2) spherical nanoparticles: Assessment of its antimicrobial and anticancer activity. *Saudi J. Biol. Sci.* **2019**, *26*, 1385−1391.
(24) Shaikh, S.; Nazam, N.; Rizvi, S. M. D.; Ahmad, K.; Baig, M. H.; Lee, E. J.; Choi, I. Mechanistic insights into the antimicrobial actions of metallic nanoparticles and their implications for multidrug resistance. *Int. J. Mol. Sci.* **2019**, *20*, 2468.
(25) Jose, M.; Sienkiewicz, P.; Szymańska, K.; Darowna, D.; Moszyński, D.; Lendzion-Bieluń, Z.; Szymański, K.; Mozia, S. Influence of preparation procedure on physicochemical and antibacterial properties of titanate nanotubes modified with silver. *Nanomaterials* **2019**, *9*, 795.
(26) Li, H.; Li, Q.; Li, Y.; Sang, X.; Yuan, H.; Zheng, B. Stannic oxide nanoparticle regulates proliferation, invasion, apoptosis, and oxidative stress of oral cancer cells. *Front. Bioeng. Biotechnol.* **2020**, *8*, 768.
(27) Tabei, Y.; Sugino, S.; Nakajima, Y.; Horie, M. Reactive oxygen species independent genotoxicity of indium tin oxide nanoparticles triggered by intracellular degradation. *Food Chem. Toxicol.* **2018**, *118*, 264−271.
(28) Liang, S. X. T.; Wong, L. S.; Lim, Y. M.; Lee, P. F.; Djearamane, S. Effects of Zinc Oxide nanoparticles on Streptococcus pyogenes. *S. Afr. J. Chem. Eng.* **2020**, *34*, 63−71.
(29) Ifeanyichukwu, U. L.; Fayemi, O. E.; Ateba, C. N. Green synthesis of zinc oxide nanoparticles from pomegranate (Punica granatum) extracts and characterization of their antibacterial activity. *Mol* **2020**, *25*, 4521.
(30) Hassanpour, S.; Saadati, A.; Hasanzadeh, M. pDNA conjugated with citrate capped silver nanoparticles towards ultrasensitive bioassay of haemophilus influenza in human biofluids: A novel optical biosensor. *J. Pharm. Biomed. Anal.* **2020**, *180*, 113050.
(31) Vinoth, S.; Shankar, S. G.; Gurusaravanan, P.; Janani, B.; Devi, J. K. Anti-larvicidal activity of silver nanoparticles synthesized from Sargassum polycystum against mosquito vectors. *J. Cluster Sci.* **2019**, *30*, 171−180.
(32) Hussein, R. A.; El-Anssary, A. A. Plants secondary metabolites: the key drivers of the pharmacological actions of medicinal plants. *Herbal Medicine*; IntechOpen, 2019; Vol. *1*.
(33) Kuropakornpong, P.; Itharat, A.; Panthong, S.; Sireeratawong, S.; Ooraikul, B. In vitro and in vivo anti-inflammatory activities of Benjakul: a potential medicinal product from Thai traditional medicine. *Evid. Based Complement Alternat. Med.* **2020**, *2020*, 9760948.
(34) Ahmad, A.; Abuzinadah, M. F.; Alkreathy, H. M.; Banaganapalli, B.; Mujeeb, M. Ursolic acid rich Ocimum sanctum L leaf extract loaded nanostructured lipid carriers ameliorate adjuvant induced arthritis in rats by inhibition of COX-1, COX-2, TNF-α and IL-1: Pharmacological and docking studies. *PLoS One* **2018**, *13*, No. e0193451.
(35) Singh, B. P.; Rateb, M. E.; Rodriguez-Couto, S.; Polizeli, M. D. L. T. D. M.; Li, W.-J. Microbial secondary metabolites: recent developments and technological challenges. *Front. Microbiol.* **2019**, *10*, 914.
(36) Jain, A.; Anitha, R.; Rajeshkumar, S. J. R. J. Anti inflammatory activity of Silver nanoparticles synthesised using Cumin oil. *Res. J. Pharm. Technol.* **2019**, *12*, 2790−2793.
(37) Khalil, A. T.; Ayaz, M.; Ovais, M.; Wadood, A.; Ali, M.; Shinwari, Z. K.; Maaza, M. In vitro cholinesterase enzymes inhibitory potential and in silico molecular docking studies of biogenic metal oxides nanoparticles. *Inorg. Nano-Met. Chem.* **2018**, *48*, 441−448.
(38) Zhao, T.; Ding, K.-M.; Zhang, L.; Cheng, X.-M.; Wang, C.-H.; Wang, Z.-T. Acetylcholinesterase and butyrylcholinesterase inhibitory activities of β-carboline and quinoline alkaloids derivatives from the plants of genus Peganum. *J. Chem.* **2013**, *2013*, 717232.
(39) Li, S.; Li, A. J.; Travers, J.; Xu, T.; Sakamuru, S.; Klumpp-Thomas, C.; Huang, R.; Xia, M. Identification of compounds for butyrylcholinesterase inhibition. *SLAS Discovery* **2021**, *26*, 1355−1364.
(40) Sahin, K.; Zengin Kurt, B.; Sonmez, F.; Durdagi, S. Novel AChE and BChE inhibitors using combined virtual screening, text

https://doi.org/10.1021/acsomega.3c02932
ACS Omega 2023, 8, 27439−27449

mining and in vitro binding assays. *J. Biomol. Struct. Dyn.* **2020**, *38*, 3342−3358.
(41) Jiratchayamaethasakul, C.; Ding, Y.; Hwang, O.; Im, S. T.; Jang, Y.; Myung, S. W.; Lee, J. M.; Kim, H. S.; Ko, S. C.; Lee, S. H. In vitro screening of elastase, collagenase, hyaluronidase, and tyrosinase inhibitory and antioxidant activities of 22 halophyte plant extracts for novel cosmeceuticals. *Fish. Aquat. Sci.* **2020**, *23*, 6.
(42) Liyanaarachchi, G. D.; Samarasekera, J. K. R. R.; Mahanama, K. R. R.; Hemalal, K. D. P. Tyrosinase, elastase, hyaluronidase, inhibitory and antioxidant activity of Sri Lankan medicinal plants for novel cosmeceuticals. *Ind. Crops Prod.* **2018**, *111*, 597−605.
(43) Boran, R. Investigations of anti-aging potential of Hypericum origanifolium Willd. for skincare formulations. *Ind. Crops Prod.* **2018**, *118*, 290−295.
(44) Luo, J.; Mills, K.; le Cessie, S.; Noordam, R.; van Heemst, D. Ageing, age-related diseases and oxidative stress: what to do next? *Ageing Res. Rev.* **2020**, *57*, 100982.
(45) Olson, L. C.; Redden, J. T.; Schwartz, Z.; Cohen, D. J.; McClure, M. J. Advanced glycation end-products in skeletal muscle aging. *Bioengineering* **2021**, *8*, 168.
(46) Thakur, B.; Kumar, A.; Kumar, D. Green synthesis of titanium dioxide nanoparticles using Azadirachta indica leaf extract and evaluation of their antibacterial activity. *South Afr. J. Bot.* **2019**, *124*, 223−227.
(47) Faisal, S.; Jan, H.; Shah, S. A.; Shah, S.; Khan, A.; Akbar, M. T.; Rizwan, M.; Jan, F.; WajidullahAkhtar, N.; Akhtar, N.; et al. Green synthesis of zinc oxide (ZnO) nanoparticles using aqueous fruit extracts of Myristica fragrans: their characterizations and biological and environmental applications. *ACS Omega* **2021**, *6*, 9709−9722.
(48) Jan, H.; Khan, M. A.; Usman, H.; Shah, M.; Ansir, R.; Faisal, S.; Ullah, N.; Rahman, L. The Aquilegia pubiflora (Himalayan columbine) mediated synthesis of nanoceria for diverse biomedical applications. *RSC Adv.* **2020**, *10*, 19219−19231.
(49) Faisal, S.; Khan, M. A.; Jan, H.; Shah, S. A.; Abdullah; Shah, S.; Rizwan, M.; Wajidullah; Akbar, M. T.; Redaina. Edible mushroom (Flammulina velutipes) as biosource for silver nanoparticles: from synthesis to diverse biomedical and environmental applications. *Nanotech* **2020**, *32*, 065101.
(50) Hombach, M.; Jetter, M.; Blöchliger, N.; Kolesnik-Goldmann, N.; Böttger, E. C. Fully automated disc diffusion for rapid antibiotic susceptibility test results: a proof-of-principle study. *J. Antimicrob. Chemother.* **2017**, *72*, 1659−1668.
(51) Garibo, D.; Borbón-Nuñez, H. A.; de León, J. N. D.; García Mendoza, E.; Estrada, I.; Toledano-Magaña, Y.; Tiznado, H.; Ovalle-Marroquin, M.; Soto-Ramos, A. G.; Blanco, A.; Rodríguez, J. A.; et al. Green synthesis of silver nanoparticles using Lysiloma acapulcensis exhibit high-antimicrobial activity. *Sci. Rep.* **2020**, *10*, 12805.
(52) Imran, M.; Jan, H.; Faisal, S.; Ali Shah, S.; Shah, S.; Naeem Khan, M.; Taj Akbar, M.; Rizwan, M.; Jan, F.; Syed, S. In vitro examination of anti-parasitic, anti-Alzheimer, insecticidal and cytotoxic potential of Ajuga bracteosa Wallich leaves extracts. *Saudi J. Biol. Sci.* **2021**, *28*, 3031−3036.
(53) Jan, H.; Shah, M.; Andleeb, A.; Faisal, S.; Khattak, A.; Rizwan, M.; Drouet, S.; Hano, C.; Abbasi, B. H. Plant-based synthesis of zinc oxide nanoparticles (ZnO-NPs) using aqueous leaf extract of aquilegia pubiflora: Their antiproliferative activity against HepG2 cells inducing reactive oxygen species and other in vitro properties. *Oxid. Med. Cell. Longevity* **2021**, *2021*, 4786227.
(54) Jan, H.; Zaman, G.; Usman, H.; Ansir, R.; Drouet, S.; Gigliolo-Guivarc'h, N.; Hano, C.; Abbasi, B. H. Biogenically proficient synthesis and characterization of silver nanoparticles (Ag-NPs) employing aqueous extract of Aquilegia pubiflora along with their in vitro antimicrobial, anti-cancer and other biological applications. *J. Mater. Res. Technol.* **2021**, *15*, 950−968.
(55) Jan, H.; Usman, H.; Shah, M.; Zaman, G.; Mushtaq, S.; Drouet, S.; Hano, C.; Abbasi, B. H. Phytochemical analysis and versatile in vitro evaluation of antimicrobial, cytotoxic and enzyme inhibition potential of different extracts of traditionally used Aquilegia pubiflora Wall. Ex Royle. *BMC Complementary Med. Ther.* **2021**, *21*, 165.
(56) Faisal, S.; Abdullah; Jan, H.; Shah, S.; Shah, S.; Rizwan, M.; Zaman, N.; Hussain, Z.; Uddin, M. N.; Bibi, N.; Khattak, A.; et al. Bio-catalytic activity of novel Mentha arvensis intervened biocompatible magnesium oxide nanomaterials. *Catalysts* **2021**, *11*, 780.
(57) Shah, M.; Nawaz, S.; Jan, H.; Uddin, N.; Ali, A.; Anjum, S.; Giglioli-Guivarc'h, N.; Hano, C.; Abbasi, B. H. Synthesis of bio-mediated silver nanoparticles from Silybum marianum and their biological and clinical activities. *Mater. Sci. Eng. C* **2020**, *112*, 110889.

https://doi.org/10.1021/acsomega.3c02932
ACS Omega 2023, 8, 27439−27449